



1 Surface deposition of marine fog and its treatment in the WRF model

2

3 Peter A. Taylor¹, Zheqi Chen¹, Li Cheng¹, Soudeh Afsharian¹, Wensong Weng¹, George A.
4 Isaac^{1,2}, Terry W. Bullock³, Yongsheng Chen¹

5

6 ¹ Centre for Research in Earth and Space Science, Lassonde School of Engineering, York University, Toronto,
7 Ontario, M3J 1P3, Canada

8 ² Weather Impacts Consulting Incorporated, 20 Pine Ridge Trail, Barrie, Ontario, L4M 4Y8, Canada

9 ³ Met-Ocean & Digital Environment Solutions, 133 Crosbie Road, St. John's, NL, A1B 4A5, Canada

10

11 *Correspondence to:* Peter Taylor (pat@yorku.ca)

12

13

14

15

16 **Abstract** There have been many studies of marine fog, some using WRF and other models. Several model studies
17 report over-predictions of near surface liquid water content (Q_c) leading to visibility estimates that are too low. This
18 study has found the same. One possible cause of this overestimation could be the treatment of a surface deposition
19 rate of fog droplets at the underlying water surface. Most models, including the Advanced Research Weather
20 Research and Forecasting (WRF-ARW) Model, available from the National Center for Atmospheric Research
21 (NCAR), take account of gravitational settling of cloud droplets throughout the domain and at the surface. However,
22 there should be an additional deposition as turbulence causes fog droplets to collide and coalesce with the water
23 surface. A water surface, or any wet surface, can then be an effective sink for fog water droplets. This process can be
24 parameterized as an additional deposition velocity with a model that could be based on a roughness length for water
25 droplets, z_{0c} , that may be significantly larger than the roughness length for water vapour, z_{0q} . This can be
26 implemented in WRF either as a variant of the Katata scheme for deposition to vegetation, or via direct
27 modifications in boundary-layer modules.

28

29 1. Introduction

30 This study was initiated when it was found that predicting fog in areas offshore from Atlantic Canada using the
31 NCAR/UCAR Weather Research and Forecasting model (WRF-ARW) was generally satisfactory in terms of fog
32 occurrence but gave high values of cloud water mixing ratio leading to visibilities that were too low compared to
33 observations. Other studies of marine fog had encountered similar problems (e.g. Chen et al 2020). Koraćin et al
34 (2014) had noted "From the many modeling studies of sea fog, essentially numerical experiments/ simulations/
35 forecasting that started in the immediate post WWII period, it becomes clear that deterministic forecasting of sea fog
36 onset and its duration has generally been unsuccessful.". On land and over the sea the formation and decay of fog in
37 the atmospheric boundary layer is a complex issue involving many processes including cloud microphysics, long
38 wave and solar radiation, turbulent boundary layer mixing, advection and surface interactions. Modelling of fog, in
39 idealized one dimensional or single column models up to operational 3-D weather prediction and climate models is a
40 challenge which many have addressed over the years, as noted by Koraćin (2017), Gulpepe et al (2017) and many
41 others. Koraćin et al (2014) review marine fog processes and studies up to 2014, noting the importance of air-sea
interactions. They discuss fog water deposition to vegetation extensively but not turbulent deposition to water



42 surfaces, and it is missing from their Fig 1 (and Fig 9.1 in Koraćin 2017) showing " the main processes governing
43 the formation, evolution, and dissipation of marine fog". Although fog could be caused by mixing two slightly sub-
44 saturated air parcels and causing saturation due to curvature of the saturated mixing ratio versus temperature line,
45 most fog formation is initialized by cooling the lower parts of a column of moist, but unsaturated, air. This can arise
46 because of long wave radiative heat loss from the underlying surface (radiation fog), vertical displacement of the air
47 column as it travels over sloping terrain or horizontal advection over a cooler surface. Our focus is on the advection
48 fog situation over ocean waters, a frequent occurrence over areas such as the Grand Banks and offshore areas of
49 Eastern Canada as the wind blows moist air from over the Gulf Stream towards the Labrador current (Taylor 1917;
50 Isaac et al 2020).

51

52 **1.1 Fog and the underlying surface**

53 The focus in this paper is on the interactions of fog water droplets with the underlying water surface, how this is
54 being modelled, how it could be improved in the widely used WRF model, and to briefly suggest some field
55 measurements to support this work. The basic hypothesis will be that, in addition to gravitational settling, turbulence
56 will induce collisions between fog droplets and the water surface and that most of these collisions will lead to
57 coalescence, so that the water surface is a sink for water droplets. This can be represented in terms of a deposition
58 velocity, over and above the settling or terminal velocity associated with small cloud droplets falling through air
59 under gravity and predictable assuming Stokes law (see, for example, Rogers and Yau 1989). If there is an
60 enhanced turbulent deposition to the surface one would then expect the cloud droplet mixing ratio (Q_c) to increase
61 with height (z) above the surface, at which Q_c would approach zero. In a constant flux layer this would lead to a
62 logarithmic profile and allow the concept of a roughness length for cloud droplets, z_{0c} , although the profile can be
63 modified to incorporate gravitational settling. Not included is the possible creation of spray droplets by breaking
64 waves in high wind speeds, and this may need consideration in high seas with strong winds.

65

66 There have been many studies on the collision and coalescence of raindrops and cloud droplets, and of droplets
67 impacting hydrophobic surfaces but relatively few concerning interactions between cloud or fog droplets and ocean
68 surfaces. Over water the combination of wind and waves will lead to impacts occurring at a range of speeds and
69 incidence angles and relatively little is known about the details of this important interaction. The paper by Hallett
70 and Christensen (1984) and the reference to it by Isaac and Hallett (2005), although primarily on impacts at normal
71 incidence, do however support our expectation that fog droplets interacting with the ocean surface are likely to
72 coalesce eventually even if they may bounce on initial impact if that occurs at a shallow angle. If fog droplets do
73 collide with the underlying surface, whether it is the ocean, a lake, a water puddle on land or wet vegetation one
74 would expect coalescence and deposition of the fog droplets to the surface. Gravitational settling will play a role in
75 this but droplet impacts on the surface due to turbulence also need to be considered. As a result of deposition there
76 would be a reduction in the fog/cloud water mixing ratio (Q_c), maybe to zero, at the lower boundary which would
77 lead to a positive value for dQ_c/dz and a downward flux of Q_c .

78



79 1.2 Aerosol and vegetation

80 If we broaden our view and consider aerosols in general, we find that significant work has been done in the same
81 size range as fog droplets (1-50 μm). Recent reviews by Emerson et al (2020) and Farmer et al (2021) make it very
82 clear that dry deposition (i.e. not rainfall related) of aerosol particles, solid or liquid, is a key process for their
83 removal, that it is driven by turbulence and strongly dependent on particle size. For aerosol with diameters $> 1 \mu\text{m}$
84 gravitational settling and turbulent diffusion both contribute to the overall deposition velocity. The aerosol studies
85 include both water surfaces and vegetation. It is clear from Farmer et al (2021, Fig 3) that deposition velocity, V_{dep} ,
86 over water increases significantly with aerosol diameter between 1 and 50 μm , while this variation is somewhat less
87 over other surfaces. Farmer et al's plots are not normalized by friction velocity or wind speed which probably
88 accounts for some of the variability in V_{dep} at fixed diameters.

89

90 There have been studies of fog deposition to vegetation and also to meshes designed to catch fog water (e.g. Section
91 3.4 of Gultepe et al 2017). However, as far as we are aware, the models of fog droplet deposition to water surfaces
92 have either been via gravitational settling alone, ignored, or considered as a part of a turbulent, total water (vapour,
93 q , plus liquid droplets) flux at the surface. Right at the surface the flux of water vapour will rely on molecular
94 transfer alone while collision and coalescence of water droplets can be much more efficient and requires separate
95 treatment.

96

97 2 Boundary-Layer modelling

98 For aerosols and sometimes other quantities, weather prediction, and other models tend to use deposition velocities
99 (V_{dep}) to relate fluxes to an underlying surface to concentrations at some level above the surface. From a boundary-
100 layer perspective, one often looks at the concentration profile and an eddy diffusivity. The simplest, and traditional,
101 way to model flux-profile relationships of a quantity, s , in turbulent boundary-layer flow near rough walls is via an
102 eddy viscosity/diffusivity, $K_s(z) = k u^* (z + z_{0s})$, where k is the Karman constant (0.4) and u^* is the friction velocity. The
103 roughness length, z_{0s} , is specific to the property (horizontal velocity, temperature, mixing ratio ...) under
104 consideration and will vary considerably depending on the physics of the final transfer process at the surface. The
105 traditional way to determine z_{0s} is to consider an approximately constant flux layer near the surface - leading to a
106 logarithmic profile,

$$107 \quad S - S_0 \approx (s^*/k) \log(z/z_{0s}), \quad (1)$$

108 where S_0 is the surface value. This will imply that $S = S_0$ at $z = z_{0s}$ and is the empirical way in which z_{0s} can be
109 determined. It is well known, see for example Garratt (1992, p 89) or Brutsaert (1982, p 121) that roughness lengths
110 for momentum (z_{0m}) and heat or water vapour (z_{0T} , z_{0q}) transfers differ because form drag on roughness elements is
111 the major cause of momentum transfer while molecular diffusivity at the surface is needed to effect heat transfer. As
112 a result, $z_{0m} \gg z_{0q}$, except maybe over very smooth aerodynamically smooth surfaces. We will propose the use of
113 z_{0c} for cloud droplet collision and coalescence with the water surface. We have no measurement data to determine a
114 value, which might well vary with droplet size and sea state but can use reported aerosol studies to provide some
115 guidance. We do however expect that $z_{0c} \gg z_{0q}$.



116
117 If the fog has continued for some time one might expect that the relative humidity, $RH = 100\%$ in the fog layer, with
118 no significant condensation or evaporation. There will then be a near steady state in the lower fog layers with
119 constant downward Q_c flux (F_{Q_c}). This flux will be a combination of turbulent diffusion and gravitational settling
120 ($w_s Q_c$) where w_s is the gravitational settling velocity, based on Stokes law. If, as we will assume, $Q_c \rightarrow 0$ as $z \rightarrow 0$
121 then turbulent transfer will dominate as the surface is approached and logarithmic Q_c profiles should result.
122 In our model calculations, with an eddy diffusivity, $K_c(z) = ku^*(z+z_{0c})$, we find $RH \approx 100\%$ in the fog layers,
123 typically up to around 100m, and see constant flux layers with near-logarithmic Q_c profiles through most of this
124 height range, as in Fig 4. Departures from logarithmic are due in part to the effects of gravitational settling which
125 accounts for part of the downward flux.

126
127 Marine fog in the areas under consideration is often in moderate and high wind conditions (Isaac et al, 2020) and
128 relatively low heights ($< 10\text{m}$) are used as the lowest model level. In that lowest, constant flux, "wall" layer with
129 neutral stratification, we can assume horizontal homogeneity, a constant downward flux of Q_c and a steady state.
130 We can then seek the solution to

$$131 \quad w_s Q_c + (ku^*(z + z_{0c}) dQ_c/dz = F_{Q_c} = u^*q_c^*, \quad (2)$$

132 where F_{Q_c} is a downward flux of cloud droplet liquid water mixing ratio. With $Q_c = Q_{c0}$ at $z = 0$, the solution is,

$$133 \quad Q_c(z) - Q_{c0} = (u^*q_c^*/w_s) [1 - \exp(-w_s \zeta / (ku^*))], \text{ where } \zeta = \ln((z+z_{0c})/z_{0c}). \quad (3)$$

134 If w_s/u^* is small, then to first order in $w_s \zeta / (ku^*)$, (3) becomes simply

$$135 \quad Q_c(z) - Q_{c0} = (q_c^*/k) \ln((z+z_{0c})/z_{0c}), \text{ with } Q_c = Q_{c0} \text{ at } z = 0. \quad (4)$$

136 If this is used to relate z_{0c} to V_{dep} , and with $Q_{c0} = 0$ we would have

$$137 \quad V_d = u^*k / (\ln((z_1+z_{0c})/z_{0c})), \quad (5)$$

138 where z_1 is the height above the surface where Q_c is measured. This logarithmic profile approximation could be fit
139 to measured Q_c profiles to determine z_{0c} from observations. As with z_{0m} this is a somewhat empirical approach. In
140 the same way that the use of the z_{0m} concept is widely accepted without precise calculation of the form drag on
141 roughness elements we would hope that future experimental determination of z_{0c} would be a way to account for the
142 effects of turbulent collision and coalescence of fog droplets with a water surface. For radiation fog in low wind
143 speeds over land, stable air density stratification effects could be significant and can be accounted for with Monin-
144 Obukhov similarity modifications to $K_c(z, L)$ if the Obukhov length (L) can be determined.

145
146 The expected values of terminal velocity, w_s for a droplet of diameter, d , and density ρ , falling under gravity (g)
147 through air of density ρ_a and molecular viscosity, μ , should be considered. In reality the fog droplet size distribution
148 will be broad and often bimodal (see Isaac et al 2020). The two peaks in some of Isaac et al's measured PDFs are at
149 diameters near $6 \mu\text{m}$ and $25 \mu\text{m}$ with Stokes law terminal velocities ($w = g d^2 (\rho - \rho_a) / \mu$) of 0.001 ms^{-1} and 0.019 ms^{-1} .
150 These are clearly small compared to wind speed but for the larger diameter, where the bulk of the liquid water
151 content (LWC) is often measured, the terminal velocity corresponds to 67 m per hour and will represent a
152 considerable removal rate in fog which may last several days. The key parameter in our constant flux with



153 gravitational settling model is $S = w_s/k u^*$. In moderate winds over the ocean one might expect u^* values in the 0.1-
154 0.5 ms^{-1} range, $k = 0.4$ and so the parameter, S will generally be in the range 0.006 to 0.46 while ζ may be 5-10 at the
155 lowest grid point, implying that gravitational settling can play a significant role and that Eq. (3) may provide a more
156 appropriate profile for the larger droplets. In principle Eq. (3) should be used to refine any z_{0c} estimates from
157 measurements. For typical friction velocities ($0.1 - 0.5 \text{ ms}^{-1}$) and with the lowest model level at $z_l = 1.7 \text{ m}$ with $z_{0c} =$
158 0.01 or 0.001 m , V_d values would be in the range 0.005 to 0.04 ms^{-1} , quite comparable with the gravitational settling
159 velocities so both will play a role in the modelling of deposition to the surface.

160
161 Ideally values for z_{0c} would be established from field measurements BUT we are not aware of any height profiles of
162 Q_c in fog over water and for now will treat z_{0c} as a tuning parameter in our models. Over most land surfaces, z_{0m} is
163 considered independent of Reynolds number and we might hope that the same would apply for z_{0c} . Over water
164 surfaces with ripples and waves as the roughness elements life gets more complicated and the roughness length for
165 momentum, z_{0m} , can be wind speed dependent, governed by the Charnock-Ellison relationship¹ (Charnock 1955),
166 $z_{0m} = a u^{*2} / g$, where a is referred to as Charnock's constant, with typical values in the $0.01 - 0.03$ range. Establishing
167 precise over water values for z_{0c} will prove at least as difficult as for z_{0m} , noting that it may also vary with droplet
168 size, but it does provide a framework for representing this potentially important fog deposition process.

169

170 **3. Past Field and Laboratory Measurements**

171 There have been many field measurements in marine fog, including, notably, G.I. Taylor's (1917) work over the
172 Grand Banks, and more recently the C-Fog study reported by Fernando et al (2021). As far as we are aware none
173 have provided the $Q_c(z)$ profile data from which we could make z_{0c} determinations.

174

175 Over land there are some multi-level Q_c measurements indicating lower values near ground than above. Also lower
176 droplet numbers. Kunkel (1984) reports measurements of advection fog in July 1980 and July 1981, at 2 levels (5m
177 and 30m) on a tower "in the middle of a large, flat, open area" about 12 km inland from the Atlantic on Cape Cod.
178 There is some variability but his liquid water content values (W , gm^{-3}) are always higher at 30m than at 5m and the
179 ratios are generally between 2 and 3. There are some differences in droplet size between the levels but they are
180 relatively modest and less consistent. Ignoring stratification effects, assuming that a logarithmic profile is
181 appropriate and that $Q_{c0} = 0$ then the ratios of 2 and 3 in Q_c correspond to z_{0c} values of 0.833 m and 2.04 m. If Q_{c0}
182 were > 0 , say some fraction of $Q_c(5\text{m})$, then the z_{0c} values would be higher. Pinnick et al (1978) report Q_c
183 measurements, from February 1976 above an inland site in Germany, at multiple heights up to 180 m with light
184 scattering instruments carried aloft by a tethered balloon. Water content was calculated from particle size
185 distributions and, from their photographs, the local land surface appears open and flat. Their sample profiles, in fog
186 and haze, generally show Q_c increasing with height and 3 of 4 cases shown are consistent with increases by factors
187 of 2-3 between 5 - 30 m. Most of their results appear to be in radiation fog with light wind conditions. Klemm et al

¹ Henry Charnock always told me that Tom Ellison had suggested the dimensional analysis behind what is generally referred to as the Charnock relationship, so I refer to it in this way. - Peter Taylor



188 (2005) report eddy covariance measurements of fog water fluxes to a spruce forest at Waldstein, in a mountainous
189 area of Bavaria Germany, and compare results with related model studies. They report that "turbulent exchange
190 ...dominates over sedimentation at that site" and investigate relationships between liquid water content (LWC , gm^{-3})
191 and visibility. Their flux model is based on a deposition velocity, V_{dep} , with deposition to the canopy,
192 $F_{tot} = V_{dep} * LWC$, including both turbulent flux and gravitational settling. They note that some studies at the same
193 location (Burkhard et al, 2002) report significant differences in downward flux at different levels (flux at 22m can be
194 45% less than at 35m), perhaps illustrating the difficulty of making representative measurements close to the canopy
195 top. Evaporation of fog droplets is also cited as a possible cause of these differences. It is perhaps also worth adding
196 that fog water collectors (e.g. Schemenauer and Cereceda, 1991) can enhance the amount of fog water that is
197 removed at ground level and provide an important source of clean water for some isolated communities. a removal
198 efficiency of 20% is estimated for a 2-layer, 12m x 4m polypropylene mesh.

199
200 Turning to aerosol studies, Farmer et al (2021) provide an extensive list of laboratory and field studies of aerosol
201 deposition to both land (grassland, forest, snow and ice) and water surfaces. Many provide V_{dep} values for aerosols in
202 our size range. Deposition velocity measurements in wind tunnel studies in a short report by Schmel and Sutter
203 (1974) are interesting, but lack details of how the aerosol flux to the surface was determined. From their Fig 3 we
204 can estimate average deposition velocities for selected particle sizes and wind speeds. Unfortunately, it is not clear
205 at what heights their wind speeds were measured and their z_{0m} and u^* values are somewhat suspect. If we assume
206 that $z_{0m} = 0.0002$ m and that wind speeds in their tunnel were measured at a height of 0.1 m then their average U (7.2
207 ms^{-1}) and u^* (0.44ms^{-1}) values are reasonably consistent and their V_{dep} value of 0.04ms^{-1} for $6 \mu\text{m}$ diameter aerosol
208 would lead to $z_{0c} \sim 10^{-4}$ m. For larger diameter aerosol ($28 \mu\text{m}$) $V_{dep} = 0.37 \text{ms}^{-1}$ and $z_{0c} \sim 0.062$ m with the same
209 wind assumptions, suggesting strong size effects, but we are wary of suggesting precise values.

210
211 Field data studies in the Farmer et al (2021) list include studies on Lake Michigan by Caffrey et al (1998) and Zufall
212 et al (1998) with deposition to surrogate surfaces, and a recent report by Qi et al (2020) from the NW Pacific Ocean.
213 These and other papers confirm the strong size dependence of deposition velocity and acknowledge wind speed
214 dependence but are often concerned with long term estimates of the deposition of chemical species to the ocean or
215 lake rather than short term events. One way in which wind speed plays a role is via wave breaking and "broken"
216 water surfaces, a concept used in a model proposed by Williams (1982). This proposes that dry deposition of aerosol
217 particles is considerably different between smooth and broken patches of the water surface with a much higher
218 resistance over the smooth areas.

219
220 To briefly summarize we believe that there are observations to support the idea that the underlying land or water
221 surface can be an effective sink for fog droplets, and other, similar sized, aerosol. The deposition velocity will have
222 a dependence on droplet size, especially over water, but there is a lack of reliable data, even over land, to calibrate
223 our simple, roughness length based approach to modelling the turbulent deposition of fog droplets. Our roughness



224 length, z_{0c} , will have to remain as a tuning parameter until more extensive fog droplet profile and flux measurements
225 can be made.

226

227 **4 Model Studies**

228 As reported by Koračin (2017), there have been many studies aimed at understanding and/or predicting the
229 occurrence of fog, and Kim and Yum (2012) also provide a review focused on marine fog. For our purposes it is
230 relevant to see how different model papers discuss deposition of fog water to the surface and their surface boundary
231 conditions on Q_c . The model of Brown and Roach (1976) focusses on radiation fog, in relatively low wind speeds
232 and provides an excellent summary of the key components needed to model fog formation and its life cycle,
233 including radiation, turbulent diffusion and gravitational settling. They note that " liquid water (as well as water
234 vapour) is also lost to the ground by turbulent diffusion and gravitational settling of droplets." and their lower
235 boundary conditions include $w = 0$ for $z = 0$ and $t > 0$, where w is their liquid water mixing ratio. Brown and Roach
236 assert that " K_h , K_q , K_w , exchange coefficients for heat, water vapour and liquid water respectively" are assumed
237 equal in their model. In adiabatic conditions they state $K = kz u^*$ but avoid discussion of roughness length.
238 Extrapolating their w vs $\log z$ profiles to $w = 0$ would indicate a z_{0c} value, for liquid water, of slightly less than 10^{-2}
239 m. This is consistent with their use of the K model of Zdunkowski and Barr (1972) who set $z_0 = 1$ cm. Zdunkowski
240 and Barr's treatment of the conservation equation and lower boundary condition for M , the total moisture content
241 (vapor plus droplets), plus zero flux of M to the surface, generally leads, inappropriately, to liquid water profiles
242 with maxima at the surface. Barker (1977) developed a similar model for maritime boundary-layer fog and also uses
243 the same eddy diffusivity and roughness length for heat, water vapour and liquid water. He assumes that cloud liquid
244 water concentration (his l_0) is zero at the water surface.

245 The COBEL and COBEL-ISBA 1-D models developed in France (Bergot 1993; Bergot and Guedalia
246 1994; Bergot et al 2005), have been used successfully at Paris's Charles de Gaulle International Airport. Bergot and
247 Guedalia (1994, hereafter referred to as BG) provide details of dew and frost deposition to the underlying surface
248 and note its importance. However their dew flux is based on direct condensation of water vapour to the surface (BG
249 Eq 22) as the inverse situation of evaporation. Their liquid water (q_l) diffuses and has a gravitational settling
250 velocity (BG Eq 17, 18) but no surface condition is specified and one assumes that the only flux to the surface is
251 through gravitational settling. Few details are given on the surface boundary conditions in the latest journal
252 publications but contour plots, e.g. Fig 13c from Bergot et al (2005) generally show Q_c maxima at the surface.
253 COBEL has also been coupled with WRF (Stolaki et al 2012) and used to simulate advection-radiation fog
254 conditions at Thessaloniki's airport.

255 Bott and Trautmann (2002) proposed PAFOG as "a new efficient model of radiation fog" and it has been
256 used by others, including, recently, and coupled to WRF, in a study by Kim et al (2020). PAFOG is a 1- dimensional
257 (z, t) model developed as a more practical version of the more complete MIFOG model (Bott et al 1990) which
258 carries multiple aerosol and size bins for fog droplets. The MIFOG model includes dynamics and thermodynamics
259 but focusses on interactions of radiation (solar and long wave) with fog droplets of varying size. The cloud droplets
260 that evolve in the model have a bimodal size distribution which varies with time with large droplets descending



261 under gravity, and being removed at the surface, at a faster rate than the small ones. The dynamics include turbulent
262 mixing via eddy diffusivities for momentum and heat. Water droplet number concentrations in each size bin are also
263 subject to diffusion with the same diffusivity as heat. The diffusivities are given by Forkel et al (1987). It appears
264 that a common roughness length, $z_0 = 0.05\text{m}$, is used for momentum, heat and water droplets. No boundary
265 conditions are given in Bott et al (1990) but from the results presented it would appear that there is no turbulent flux
266 to the surface, only deposition via gravitational settling in MIFOG. The same appears to be true with PAFOG apart
267 from possible removal of cloud water by vegetation as described by Siebert et al (1992a,b). PAFOG appears to give
268 good results for 2-m visibility (Bott and Trautmann 2002, Fig. 1). Their Fig. 2 generally shows high Q_c values (0.2,
269 0.3 g kg^{-1}) extending almost down to the surface but with a sudden drop near $z = 0$ in 3 of the 4 contour figures
270 shown. There is similar near-surface behavior of Q_c in Siebert's results but it is not clear why. All of the above
271 papers have a lack of detail on surface boundary conditions.

272 Shuttleworth (1977) and later Lovett (1984) were early modelers of fog deposition to vegetation, using
273 resistance concepts ($1/V_d$). Katata et al (2008) later developed a land surface model (mod-SOLVEG) including fog
274 and cloud water deposition on vegetation and on forests. The downward flux of cloud water is due to both turbulent
275 mixing and gravitational settling (Katata 2014) and Katata et al (2008) successfully compare their model predictions
276 with field measurements from a forest site near Waldstein in Germany. The turbulent fluxes use a vertical eddy
277 diffusivity, K_z , and multiple vegetation levels are involved. They claim that their model results compare well in
278 comparison with Klemm et al.'s (2005) application of the Lovett (1984) model. Lovett points out that there can be
279 "turbulent transfer of cloud droplets to the canopy" and that, in windy conditions "inertial impaction is the dominant
280 mechanism". These model papers all deal with forests and Katata et al (2011) describe the implementation of the
281 ideas within WRF using the MYNN 2.5 Planetary Boundary Layer scheme and WSM6 cloud microphysics. The
282 central assumption is that, within, what Katata et al (2011) call org-WRF, fog water deposition to the surface can be
283 represented as,

$$284 \quad F_{Q_c} = C_h |\underline{U}| \rho Q_c = V_d \rho Q_c \quad (6)$$

285 where \underline{U} is the wind vector at the lowest model level and ρ is air density. C_h is a bulk transfer coefficient for height h
286 above the surface (specifically the lowest model level, although h was later defined as the canopy height), V_d is a
287 deposition velocity, associated with turbulent diffusion but including gravitational settling. In what Katata et al
288 (2011) call fog-WRF the deposition velocity is set to

$$289 \quad V_d = A|U|, \text{ where } A = 0.0164(LAI/h)^{0.5}, \quad (7)$$

290 Here LAI is leaf area index (m^2 per m^2) and here h is canopy height (in m), so that the coefficient 0.0164 has units of
291 $\text{m}^{0.5}$. Values given for A in Katata et al (2008) for both needle leaf and broad leaf trees are mostly in the range 0.02 -
292 0.04, with U measured "over the canopy". If the U and Q_c measurement height was at 10 m, $Q_c(z_{0c}) = 0$ and $z_0 = z_{0c}$
293 $= 0.1\text{m}$ then, from Eq (2) and the log wind profile, $A = 0.0075$, but with $z_0 = z_{0c} = 1\text{ m}$ the result is $A = 0.03$, in the
294 middle of Katata's range.

295 Recent papers by Wainwright and Richter (2021) and Richter et al (2021) focus on marine fog using a large
296 eddy simulation model, following on from the work of Maronga and Bosveld (2017) and Schwenkel and Maronga
297 (2019, 2020) on LES studies of radiation fog. The marine fog models use Morrison et al (2005) microphysics. The



298 cloud water (Q_c) and cloud droplet number (N_c) equations include turbulent diffusion and sedimentation but there
299 seems to be no enhanced deposition to the surface. Most results (e.g. Figs 3a, 6, 10, and most of Fig. 11 from
300 Wainwright and Richter 2021) appear to show Q_c maxima at the surface although Fig.7 in Schwenkel and Maronga
301 (2019) suggests a rapid drop in Q_c near the surface. There seems to be little discussion of deposition of fog droplets
302 to the surface in most of these papers although, for their Lagrangian simulations, Richter et al (2021) note " At the
303 bottom of the domain, droplets that hit the water surface are removed from the simulation, and a new super-droplet
304 is immediately introduced randomly in the domain according to the same procedure for initialization." It is not clear
305 what this does in terms of a flux to the surface but their results (Fig 3 of their paper) in a simulation of advection fog
306 show number densities that are maximum at the fog top, around 30 m after 10 h, while Q_c and mean droplet radius
307 are maximum near the ground.

308 None of the papers that we have found use the z_{0c} approach that we have adopted, although the resistance
309 and deposition velocity ideas of Lovett (1984) and Katata et al (2008) are closely related. When roughness lengths
310 are used, the values for Q_c always appear to be the same as for water vapour.

311

312 **4. Operational NWP models**

313 Fog forecasts have been a challenge for operational NWP models as indicated by many authors including Wilkinson
314 et al (2013) who note the Gultepe et al (2006) opinion that " most NWP models were unable to provide accurate
315 visibility forecasts, unless they accounted for both liquid water content and droplet number." We also note the
316 comment of Bergot et al (2007), "Current NWP models poorly forecast the life cycle of fog, and improved NWP
317 models are needed before improving the prediction of fog".

318 Wilkinson et al (2013) focus on the droplet number issue and, in a somewhat "ad hoc" fashion, the UK Met
319 Office Unified Model at that time applied "a taper curve for cloud droplets near the surface." This reduces droplet
320 numbers between the surface and 150m without changing liquid water concentration. Droplets are then larger, have
321 higher settling velocities and so " the impact ... is greatest closest to the surface, where they increase the amount of
322 (Q_c) removed from the lowest model levels." It seemed to work but their "taper curve" approach could certainly be
323 considered somewhat "unphysical".

324 Yang et al (2010) made an evaluation on the Canadian GEM-LAM model for marine fog off the east coast
325 of Canada with nesting down to 2.5 km, using both visibility reports and Q_c comparisons with observed
326 measurements from the FRAM project (Gultepe et al 2009). Three case studies are presented with the overall
327 conclusion that GEM-LAM forecasts at 2.5 km resolution underestimate Q_c and had a warm and dry mean bias at
328 the lowest model level. This is opposite to our WRF studies which predict high Q_c values at low levels. An earlier
329 evaluation by de la Fuente et al (2007) had reported that, "... It has been shown that the current operational 15 km
330 regional GEM forecast is insufficient for forecasting (sea) fog." The GEM-HRDPS (Milbrandt et al 2016) uses a
331 MoisTKE treatment of the boundary layer which is described in Belair et al (2005). It works with the variable $q_w =$
332 $q_v + q_c$, where q_c is the total cloud water content (droplets + ice fragments) which is mixed vertically using an eddy
333 diffusivity K_H , as for heat. Assuming that surface transfers are of q_w this suggests no special treatment of cloud
334 droplets over water surfaces. Milbrandt et al (2016) indicate that the cloud microphysics then used in GEM-HRDPS



335 were based on MY2, the two-moment bulk microphysics scheme described in Milbrandt and Yau (2005). That paper
336 includes the statement "... because cloud droplets are assumed to have negligible terminal fall velocity." Fall speeds
337 were given for different hydrometeor categories but not for fog droplets. As discussed above, terminal velocities
338 under gravitational settling are small (mm s^{-1}), and can probably be considered negligible in a convective cloud but
339 for long lasting marine fog they can play an important role. Currently GEM-HRDPS uses P3 microphysics
340 (Morrison and Milbrandt, 2015). This includes gravitational settling of cloud droplets but there are subtle
341 distinctions between explicit and implicit q_c from the microphysics and the boundary-layer treatments and there
342 appears to be no surface flux of q_c , just a flux of q_v .

343 Teixeira (1999) reported on ECMWF successes in fog forecasting at that time with the Tiedtke (1993)
344 cloud scheme forecasting liquid water content. The Musson-Genon (1987) surface boundary-layer treatment treats
345 diffusion of total water with a low surface roughness length, but includes gravitational settling of liquid water.
346 Teixeira's conclusions include the statement " The comparison between the simulated and the observed visibility
347 shows that the onset of fog, the lowest values of visibility and the dissipation stage are properly simulated." In terms
348 of marine fog in the Grand Banks area the reanalysis data showed that "The comparison between the model's fog
349 climatology and the climatological data shows that the model is able to reproduce most of the major fog areas,
350 particularly over the ocean." The ECMWF (2020) model physics are documented at <https://www.ecmwf.int/en/elibrary/19748-part-iv-physical-processes>, with Chapter 3 giving information on interactions with the surface. As in
351 our approach their transfer coefficients involve roughness lengths. Over water they specify z_{0m} , based on the
352 Charnock-Elison relationship plus a laminar flow value based on molecular viscosity (ν), while for moisture they
353 specify $z_{0q} = \alpha_q \nu / u^*$, with $\alpha_q = 0.62$ (from Brutsaert, 1982), assuming simply molecular diffusion in a viscous
354 sublayer. It is important to note that the ECMWF model deals with total water as a conservative variable, $q_t = q + q_c$
355 + q_i , and that z_{0q} thus applies to water vapour, water droplets and ice fragments. The subscript "t" seems to be lost
356 after Eq 3.3 in the ECMWF document but we assume that in what follows from that point, e.g. in their Eq. 3.6, $q =$
357 q_t . Over land there are some adjustments but over water fluxes are proportional to $(q_n - q_{surf})$ where q_n is at the lowest
358 model level and q_{surf} is the surface value. The values of q_{surf} is set to $0.98 q_{sat}(T_{sk})$, where T_{sk} is the water surface
359 "skin" temperature, implying that surface relative humidity is close to 100% AND that $q_c \approx q_i \approx 0$. This
360 approximately agrees with our conjecture BUT the ECMWF model assumes the same z_0 for water vapour and cloud
361 droplets while our conjecture is that $z_{0c} \gg z_{0q}$. There is gravitational settling, with terminal velocities, $v_x(D)$, for rain
362 and snow (their Eq 7.20, 7.21) but not for cloud droplets.

364 In the USA there are many different forecast models but we will just consider the Rapid Refresh (RAP) and
365 High Resolution Rapid Refresh (HRRR) Models, based on WRF-ARW, (Skamarock et al 2019). These are run
366 operationally, with 13 km and 3km resolution meshes by NCEP and NOAA/ESRL Global Systems Laboratory.
367 They use the same MYNN boundary-layer and Thompson microphysics modules as in our coastal fog simulations
368 and thus may have similar limitations in depositing fog droplets over water. Going back to a statement in Zhou and
369 Du (2010), "Although one hopes that the liquid water content (LWC) at the lowest model level can be explicitly
370 used as fog, experience indicates that an LWC-only approach does not work well with the current NWP models due
371 mainly to two reasons: one is the too coarse model spatial resolution and the other is a lack of sophisticated fog



372 physics." Things have changed since then but the recent "somewhat improved" statement (including the qualifier,
373 somewhat) on visibility performance by Alexander et al (2020) can be noted.

374

375 **5. Fog deposition treatment in the WRF model with module_bl_mynn and module_sf_fogdes**

376 WRF versions 4.1.2 and 4.2.1 (<https://www2.mmm.ucar.edu/wrf/users/downloads.html>), and possibly earlier
377 versions, march forward in time with separate modules for dynamical and multiple physical processes (see
378 Skamarock et al 2019; Olson et al 2019). For the benefit of readers familiar with, or interested in, the WRF model
379 we provide some details, here, in Section 6 and in Cheng et al (2021). The WRF modules used here treat
380 gravitational settling and turbulent diffusion as separate processes and compute separate tendencies, including
381 deposition rates. Gravitational settling is included within the Thompson microphysics module and Eq. (4) is used to
382 compute deposition velocities associated with turbulent diffusion with $V_d = u^*k/(\ln((z_1+z_{0c})/z_{0c}))$, where z_1 is the first
383 Qc model level above the surface. The surface boundary layer is treated in a 1-D implicit finite difference mode with
384 tridiagonal matrices set up for turbulent kinetic energy, velocity components, potential temperature, humidity and
385 cloud liquid water Q_c . Variables are defined at the centres of grid cells with fluxes at the upper and lower
386 boundaries. For the cells adjacent to the ground the fluxes at the upper cell surface use an eddy diffusivity (K)
387 approach, which for a downward flux of cloud water is of the form $K(Q_c(2)-Q_c(1))/dz$ where $Q_c(1)$ is the value in
388 the centre of the lowest level grid cell and dz is the vertical separation. The turbulent flux to the lower boundary, in
389 this case the water surface, is computed with a deposition velocity. For cloud water the (negative) upward flux is
390 $flqc$ and is computed in module_bl_mynn as $-vdfg(Q_c(1)-sqcg)$ with the deposition velocity $V_d = vdfg$ provided by
391 module_sf_fogdes and with Q_c on the surface, $sqcg = 0$. In the unmodified module_sf_fogdes, water surfaces are
392 classified as "other" and the deposition velocity assumed is just the settling velocity of the cloud droplet falling
393 through air under gravity. In a turbulent flow over a wavy water surface the deposition velocity should also include
394 the effects of turbulence bringing droplets to impact the water surface and coalesce, and $vdfg$ should be higher.
395 There are different ways in which this can be implemented in WRF module_bl_mynn (see Cheng et al, 2021).

396

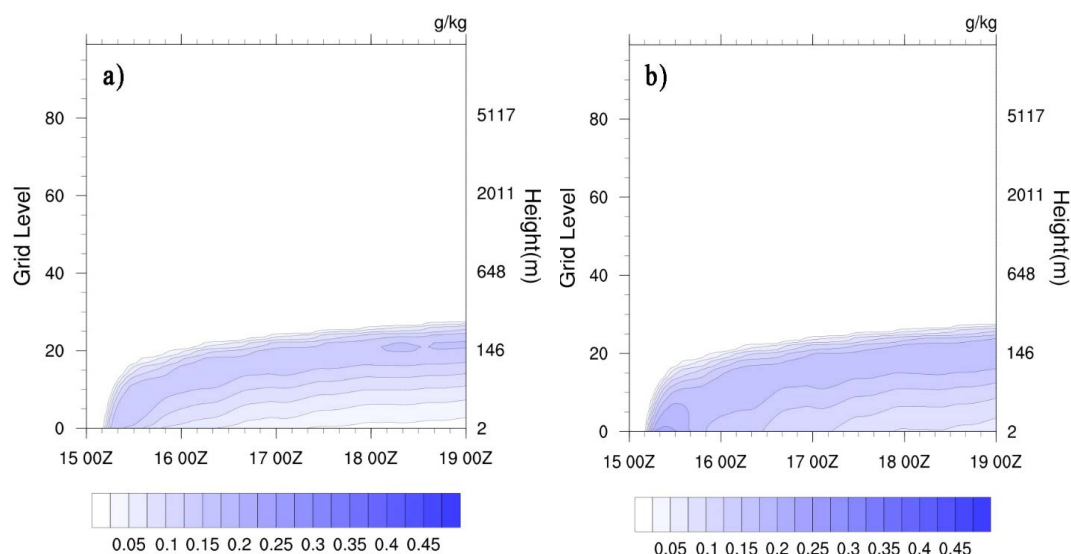
397 **6. WRF SCM set-up and tests**

398 As a basic test of our treatment of deposition of fog droplets to a water surface and for comparisons against the
399 regular WRF schemes we use the single column version of WRF (em scm xy), one of the ideal test cases described
400 by Skamarock et al (2019). In our applications of the SCM we used several boundary layer and microphysics
401 schemes, set up various vertical grids with up to 201 levels, and different lowest and upper levels. Initial soundings
402 have close to 100% relative humidity in the lowest few hundred meters, moderate wind speeds typical of the NW
403 Atlantic and WRF-SCM was typically run for 36 - 84 h. To simplify interpretation of the results, our SCM runs are
404 without any solar or long wave radiation. Surface temperatures were cooled for several hours and then held steady.
405 The main interest is to see the impact of fog droplet deposition to the underlying water surface. Physics and
406 Dynamics components of the WRF namelist input are listed in Cheng et al (2021). Turbulent deposition to the
407 surface is represented via a deposition velocity, V_d , multiplying the lowest level Q_c value at $z = z_1$. This is set as

$$408 \quad V_d = ku^*/\ln(I+z_1/z_{0c}), \quad (7)$$



409 where u^* is the friction velocity, k ($= 0.4$) is the Karman constant and z_{0c} is a roughness length specific to water
410 droplets diffusing to a water surface and coalescing. In principle it could be dependent on sea state and droplet size.
411 As noted above, roughness lengths can represent different processes for turbulent transfers of heat, water vapour,
412 momentum, and fog droplets of liquid water to the surface, and should not all be the same. Our assumption is that z_{0c}
413 (for fog/cloud droplets) should be significantly larger than z_{0q} for water vapour.
414
415 WRF-SCM was run using modules `bl_mynn`, for boundary-layer turbulent transfers, and `mp_thompson`, for cloud
416 microphysics, to generate the results shown in Figs 1-3. Since gravitational settling is represented within
417 `mp_thompson` the parameter `grav_settling` was set to 0 in `bl_mynn` (see Olson et al, 2019, section 6.4). No radiation
418 effects are included. Lack of long wave radiation will affect mixing at the top of the fog layer but we will focus on
419 lower boundary issues. In the results below the initial sounding has potential temperature of 300 K at the surface
420 increasing with height at a rate of 4 K km⁻¹. The initial relative humidity was 100 % at the surface dropping to 0 at 6
421 km. The wind profile was established with a long, no cooling run and has a geostrophic wind of (20,0) ms⁻¹. Sea
422 surface temperature was cooled at a rate of 3 K h⁻¹ for 6 h and then held fixed. The lower boundary condition
423 included a flux of water droplets to the surface, computed with a deposition velocity determined by Equation (8)
424 above and using a range of z_{0c} values.
425



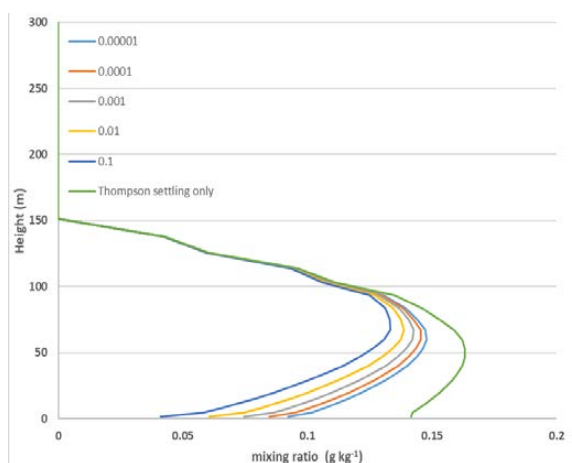
426
427
428 **Figure 1: Contours of Q_c (g kg^{-1}) generated by WRF SCM with 6h of surface cooling at 3 K h⁻¹ a) MYNN boundary layer**
429 **using the turbulence deposition scheme described with $z_{0c} = 0.01$ m plus Thompson microphysics with gravitational**
430 **settling, b) Original MYNN module with gravitational settling only in Thompson microphysics. The full vertical domain is**
431 **shown to indicate that no upper level cloud formed in these cases - it did with other input. Times on the x axis are in the**
432 **format DD HHZ, with small tic marks 4 hours apart. Run start time was 15 00Z.**



433

434 Fig. 1 shows contours of Q_c (g kg^{-1}) as it varies with (t , eta grid level) from the model calculations over 4 days
435 starting, somewhat arbitrarily, at 00Z on day 15 of a month (15 00Z) so that cooling runs to 15 06Z. Some height
436 levels are marked to indicate the grid stretching in z . These runs are for latitude 44° N (Sable Island) with 101 eta
437 grid levels. The WRF model operates with a sigma type vertical coordinate (η), decreasing from 1 at the lower
438 boundary to 0 at the upper boundary, where $p = p_t$. It has a simple form over a flat surface. Details are in Skamarock
439 et al (2019). Our model grid points are not uniformly spaced in η and the spacing increases smoothly with increasing
440 height (decreasing η). We set $p_t \approx 22000$ Pa to give a top boundary at about 12 km. The Eta levels start at $\eta = 1$ (the
441 surface) decreasing to $\eta = 0$ and $p = p_t$ at Eta level 101 (our SCM model top). In full 3D runs we take $p_t = 5000$ Pa.
442 The grid is staggered so that variables like T , Q_v , Q_c , U , V are at mid-levels while the lower boundary ($z = 0$) is at
443 the base of the lowest grid cell. Our 'grid levels' start with the centre of the lowest cell (0) and increase upwards. In Fig.
444 1a, $z_{0c} = 0.01$ m while Fig. 1b is for results with the original MYNN scheme with no surface deposition except for
445 gravitational settling in the Thompson microphysics. Fog forms as a result of the surface cooling and extends from
446 the surface to around eta level 20, which corresponds to $z \approx 150$ m. We were initially concerned by the wave-like
447 features in the contour lines. These have a period of around 17 h and arise because of inertial oscillations (of period
448 $2\pi/f$) in the wind field as it adjusts to the cooling of the surface and changing turbulent momentum transfers. They
449 decay slowly as the wind profile adjusts to the cooler surface. Values of Q_c are lower in Fig. 1a because of turbulent
450 deposition to the surface. Fig. 2 shows Q_c profiles with the MYNN boundary layer, 24 h after the start of the model
451 calculations and 18 h after the end of surface cooling. The additional turbulent deposition can play an important role
452 in lowering Q_c levels in the boundary layer while, in this case, not having a significant impact above 100m. The
453 amount of the reduction depends on the value chosen for z_{0c} .

454



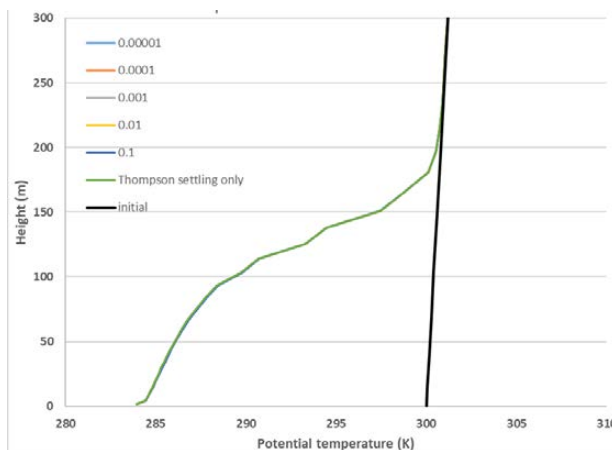
455

456

457 **Figure 2: Q_c profiles 24 h after the start of the integration and 18 h after the end of the surface cooling, by 18 K. Results**
458 **with the original MYNN (gravitational settling in Thompson microphysics only) and with a range of z_{0c} values (in m).**
459 **Time step, $dt = 60$ s, 101 levels.**



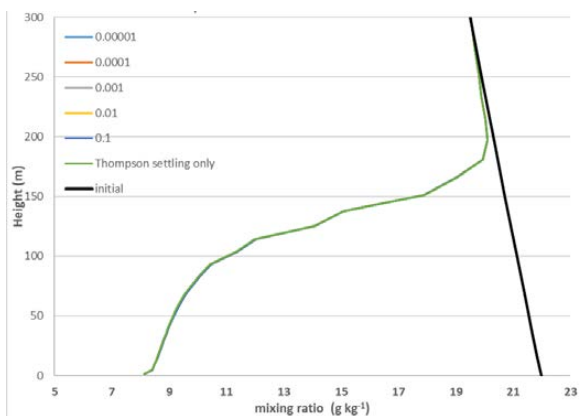
460



461

a)

462



463

b)

464

465 **Figure 3: a) Potential temperature (θ) and b) Q_v profiles corresponding to Fig. 2, including the initial profiles. Note z_{oc}**
466 **deposition of cloud droplets has minimal impact, all curves overlay.**

467

468 It is interesting to note that the removal of Q_c at the lower boundary has minimal impact on the predicted
469 temperature and water vapour, Q_v profiles (Fig. 3). It could however be important when fog starts to evaporate if the
470 air temperature rises. Note that in generating these results we have not included radiation (short wave or long wave)
471 effects in order to focus on the impacts of turbulent deposition at the water surface. Radiation can play a significant
472 role once fog has formed, and in particular long wave radiational cooling at the fog top (Yang and Gao, 2020) can
473 add to the cooling rate and can enhance turbulent mixing in the upper part of the fog layer. The center of the lowest
474 grid layer is at 1.7 m. Noting the "kinks" in the profiles at the lowest level in profiles of Q_c , Q_v and θ , we
475 investigated possible causes and plotted them on an expanded height scale (not shown). They arise because in WRF
476 modules `sf_mynn` and `sf_fogdes` the fluxes to the surface are computed with deposition velocities involving



477 $\ln((z+z_0)/z_0)$ while the eddy diffusivities used to compute fluxes at the top of the first level and levels above are
478 based on length scales proportional to kz without the z_0 addition. This will not be significant for $z \gg z_0$ but with
479 the lowest computational levels close to the surface this could be modified. This is an internal WRF issue, noted in
480 comments in the `bl_mynn` module code.

481

482 A further point from Fig 3b is that with our near saturated initial profile and strong cooling there is a significant
483 reduction in Q_v , of order 10 g kg^{-1} throughout the lowest 100 m. This will be converted to Q_c but after 24 h most
484 will have been deposited to surface, through both gravitational settling, as in the "original" curves in Fig. 2, or by a
485 combination of gravitational settling and turbulent deposition to the water surface as in the other cases shown in Fig.
486 2. In runs with gravitational settling turned off (not shown for this case but see Fig 4b) and no turbulent deposition
487 the Q_c values increase significantly, to around 6 g kg^{-1} near the surface after 12 h. Gravitation settling prevents very
488 high values from occurring but additional turbulence induced deposition further limits them.

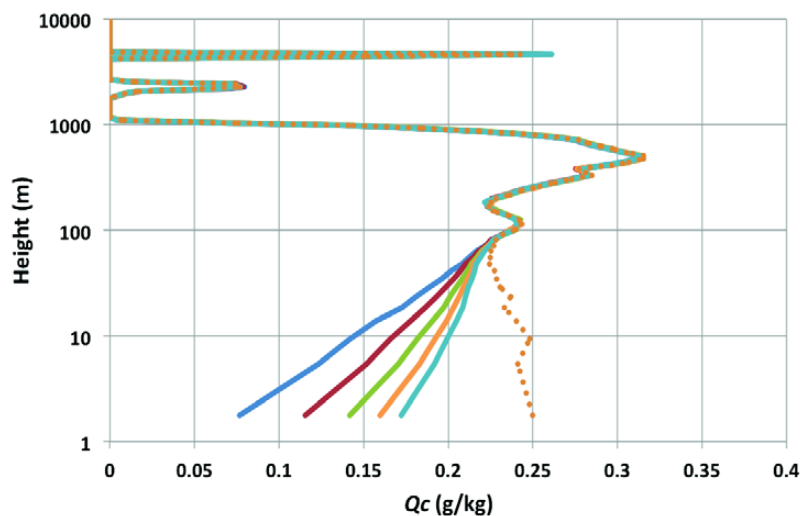
489

490 7. 3D test cases

491 Turning to the 3D WRF model we have been running the model for North Atlantic simulations for summer 2018 on
492 a domain extending from eastern Canada out beyond the Grand Banks and including Sable Island. A separate paper
493 on comparisons with visibility measurements on Sable Island is in preparation. These 3D runs have no additional
494 surface cooling and are simply run as hindcasts of the actual situation with initial and boundary conditions taken
495 from NCEP analyses. The sea surface temperatures are held fixed for daily 36 h runs, generally with a 12 h spin up.
496 Note that the input initial and boundary fields had zero Q_c . They are run with `hybrid_opt = 0`, and in the vertical
497 direction we have a straight sigma coordinate, $\eta = (p_d - p_s)/(p_t - p_s)$ with $p_t = 5000 \text{ Pa}$. Runs were also made with
498 `hybrid_opt = 2` and Q_c results were almost identical. Solar and long wave radiation can use either Goddard or
499 RRTMG scheme and we used the MYNN PBL scheme with both Thompson and the WSM6 microphysics options.
500 For details of these options see Skamarock et al (2019). Fig. 4 shows sample results from 6 h runs with the full 3D
501 model using Thompson microphysics and Goddard radiation, long and short wave. They show a similar response to
502 the SCM (Fig. 2) when turbulent deposition of cloud water to the surface is introduced. The top figure (4a) shows a
503 normal run with the Thompson microphysics module accounting for gravitational settling effects. MYNN has
504 turbulent deposition to the surface but no gravitational settling (`grav_settling = 0`). In the lower figure (4b) we
505 removed gravitational settling from the Thompson microphysics scheme (`av_c = 0`) as well as from MYNN. With no
506 turbulent deposition to the surface, and, in one special case with no gravitational settling either, there are higher Q_c
507 values as expected. These 3-D runs used NCEP analyses as initial conditions but the initial Q_c was set to zero
508 everywhere. In fog the analysis would give 100 % RH and the model then generated Q_c within a few hours but
509 without the strong temperature and Q_v drops that were simulated in our SCM tests. Gravitational settling (Fig. 4a)
510 has reduced the peak Q_c values at around 100 and 900 m from the case with no settling and the Q_c removed from
511 those levels has settled and mixed downwards to increase the Q_c values near the ground. Additional 3D runs were
512 made with the standard MYNN codes and the Katata scheme using modified deposition velocities in the "other"
513 case. These matched our results obtained with a modified MYNN code. Also, in place of the Thompson

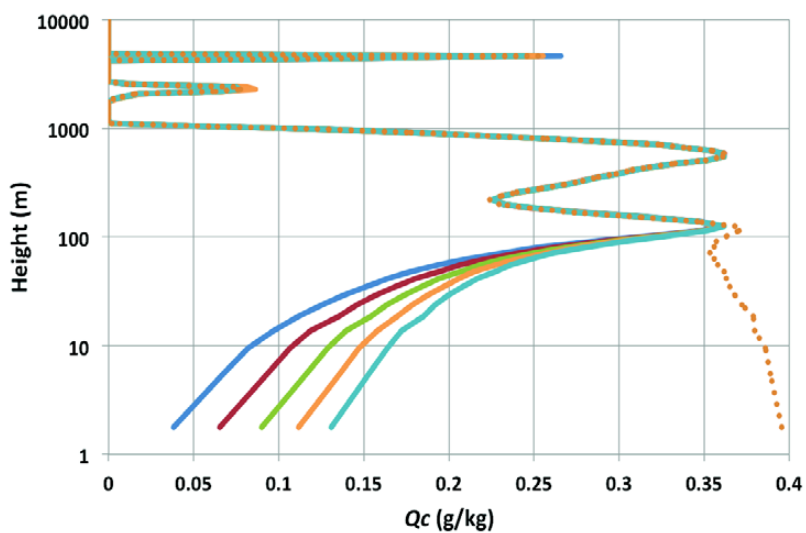


514



515 a)
516

— 0.1 — 0.01 — 0.001 — 0.0001 — 0.00001 turb deposition = 0



517 b)
518

— 0.1 — 0.01 — 0.001 — 0.0001 — 0.00001 turb deposition = 0

519 **Figure 4:** Sample 3-D WRF output at a fixed location over the Grand Banks, with different z_{0c} values (given in m) in Q_c
520 turbulent deposition, a) with and b) without gravitational settling. Start time was 7/1 12Z, 2018 and results are for 7/1
521 18Z. Results are with MYNN boundary layer and Thompson microphysics.

522



523 microphysics scheme we ran tests with WSM6 microphysics. In all cases there was a large impact of turbulent
524 surface deposition of Q_c in the lowest 100 m, even with very low values for z_{0c} . As an initial guide we suggest using
525 $z_{0c} = 0.01\text{m}$ or 0.001m as a modest value which has a solid impact. We should also emphasize that gravitational
526 settling also has an impact on Q_c values near the surface and both processes need to be included in models.

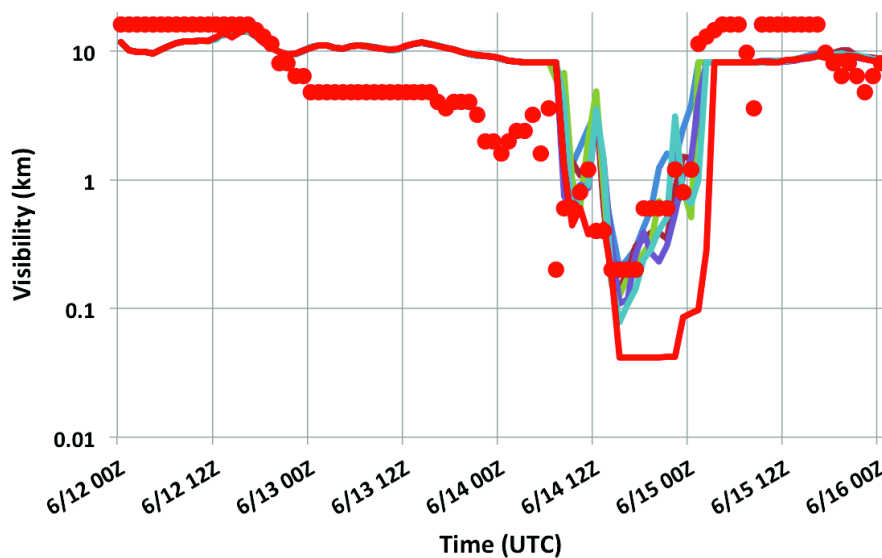
527

528 **8 Visibility considerations**

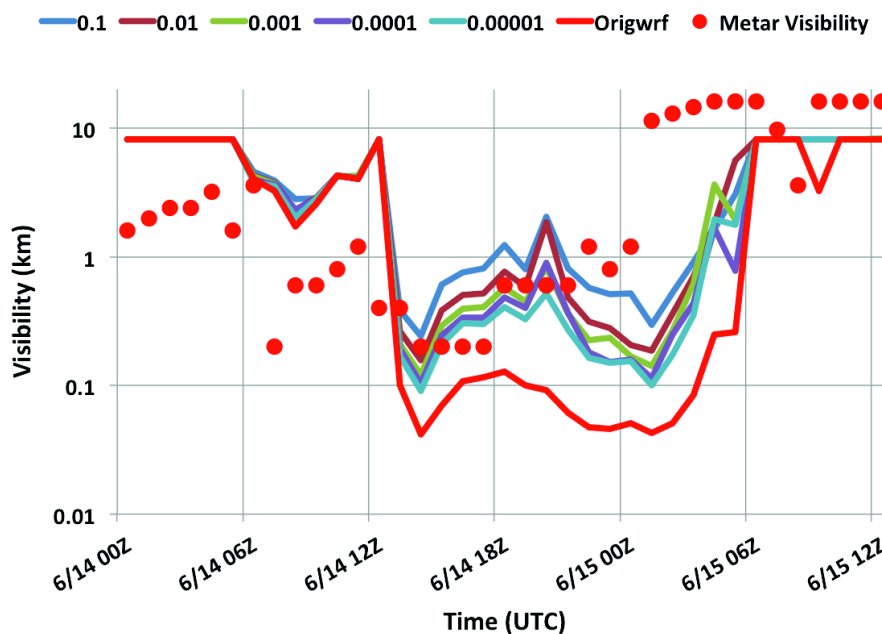
529 Models can predict liquid water mixing ratios but the critical forecast issue is visibility which will depend on the
530 number and size distribution of the fog droplets. In dense marine fog ($LWC > 0.05\text{ g m}^{-3}$), Isaac et al (2020, Fig. 12)
531 show that the size distribution of marine fog droplets is generally broad and frequently bimodal, raising concerns
532 about all simple diagnostic schemes. Despite such concerns, models such as the one proposed by Isaac et al (2020)
533 assume that visibility, or Meteorological Optical Range, MOR is proportional to liquid water density, LWC (g m^{-3} or
534 kg m^{-3}) or mixing ratio (g kg^{-1} or kg kg^{-1}), $LWC^{-2/3}$ times $N^{1/3}$ where N is the droplet number density (m^{-3}). Some
535 models include dynamic equations for N while others assume prescribed values, typically $N = 10^8\text{ m}^{-3}$. If the size
536 distribution were well known and universal this could work but as Isaac et al (2020) note the size distribution in fog
537 over the ocean can be bimodal and the number density can vary widely. In conditions with air density $\times Q_c > 0.005$
538 g m^{-3} the number density reported by Isaac et al over a site in the Grand Banks area varies between 10^7 and 3×10^8
539 m^{-3} . Medians were close to $N = 0.8 \times 10^8\text{ m}^{-3}$. Note however that these measurements were at a height of 69 m above
540 the ocean surface and if the water surface is a sink for cloud droplets one would expect lower values, and maybe a
541 different size distribution, at the WMO standard visibility measurement height of 2.5 m (WMO, 2020). Chen et al
542 (2020) note problems with too low visibility from their WRF calculations coupled to the Kunkel (1984) visibility
543 equation ($vis = -\ln(\epsilon)/\beta$ with the extinction coefficient (km^{-1}), $\beta = 144.7 W^{0.88}$ where W is in g m^{-3}). The contrast
544 threshold, ϵ was given as 0.02 by Kunkel but is set to 0.05, as recommended by the WMO (Boudala et al 2012; Chen
545 et al 2020). In the GSD algorithm used in NCEP's Unified Post Processor version 2.2, the Kunkel result is used with
546 $\epsilon = 0.02$ for visibility reductions in clouds, plus additional effects of aerosol, rainfall and humidity. The relationship
547 between visibility or MOR and Q_c or W can vary in these models between a power of $-2/3$, through -0.88 to -1 if N
548 were proportional to Q_c , but all show that too high a value of Q_c will lead to too much reduction in visibility.
549 Running standard versions of WRF one can compute visibilities with either the Isaac et al (2020) equations or the
550 GSD algorithm used in NCEP's Unified Post Processor version 2.2 (for details, see Lin et al 2017). Both led to
551 significantly lower values of MOR than were reported on Sable Island. Typical WRF values being of order $1/10$ -
552 $1/5$ of the reported visibility, suggesting Q_c values that may be high by a factor between 5 and 30. Visibility - cloud
553 water relationships are open to revision, with different values of ϵ and noting the scatter in Isaac et al's (2020) data,
554 but there is a strong suggestion that WRF values of Q_c are too high without adding additional Q_c deposition. Fig. 5
555 shows sample visibility time series computed from 3D WRF Q_c output for Sable Island, interpolated to $z = 2\text{m}$, for
556 two 36 h periods in 2018 when fog was reported at that location. Original WRF runs with just gravitational settling
557 show seriously limited visibility ($< 100\text{m}$) on some occasions when METAR visibility was closer to 1 km while
558 with added turbulent Q_c deposition and a range of z_{0c} values, the optical range was a better match to the
559 observations. These are sample cases and a more extensive comparison is planned.



560



561



562

563

564

565

Figure 5: Sample June 2018 GSD visibility hindcasts for Sable Island at 2m, using MYNN boundary layer and WSM6 microphysics, with different z_{oc} values, given in m.



566 9. Conclusions

567 It has been known for many years that fog water can be deposited on vegetation and this has been incorporated into
568 some boundary-layer fog models. It is also known that μm size aerosols can be removed from the atmosphere by
569 turbulence at water, and other, surfaces (Farmer et al, 2021). It then seems surprising that, for marine fog, turbulence
570 induced cloud/fog droplet deposition to water surfaces has not been recognised by most modellers as a significant
571 potential addition to the deposition associated with gravitational settling. Neglecting this can then lead to fog liquid
572 water mixing ratios being too high and visibility forecasts being too low. This applies to specialised boundary layer
573 models and to numerical weather prediction models. Many authors have noted the difficulties and complexity of
574 modelling fog and accurately forecasting visibility. Getting everything right will be extremely challenging but, for
575 marine fog, recognising that a significant process is missing from many models could be a step in the right direction.

576 WRF-ARW is a major contribution to the atmospheric research endeavour and the developers and
577 maintainers of this huge, multi-faceted, publicly available model deserve huge credit. As with anything of this size
578 and complexity, developed and modified over many years by many individuals, it can be very hard for new users to
579 trace through the source codes and understand just how they work. Some module codes are well documented and
580 commented, others less so. Running the model is made relatively easy, and it is designed to be robust. We have done
581 our best to understand some details and ensure that our modifications, briefly explained in Cheng et al (2021), do
582 what we expect but we make no guarantees!

583 Based on our modelling of marine fog with WRF, and reviews of the treatment of boundary layer fog in
584 WRF and other models, it seems that a much better understanding of fog droplet interaction with the ocean surface,
585 and other surfaces, is needed. Laboratory studies might be possible, and numerical simulations, but with some good
586 in situ profile measurements through fog layers over land and water one could start to better understand and
587 parameterize this process. Any foggy location on land could work but Sable Island would offer an ideal location for
588 such a study in marine fog. It is a 43 km long, narrow (mostly < 2 km wide) sand bar in the Atlantic Ocean about
589 175 km offshore from Nova Scotia, Canada. It has some vegetation, cranberry bushes and grass, wild horses and
590 many seals and is now a National Park. An upper air station (CWSA, 71600) was operated there by Environment
591 Canada until August 2019. The western tip of the island could be an ideal location for a tall mast with a variety of
592 fog related and standard meteorological research instrumentation at multiple levels. Observations
593 (https://climate.weather.gc.ca/climate_normals/index_e.html) show more than 200 (out of 720) hours of fog
594 (visibility < 1 km) on Sable Island in the months of June and July. Taylor et al (1993) made use of Sable Island as
595 an accessible offshore platform to study frontal passages over the sea in winter during the Canadian Atlantic Storms
596 Program (CASP 86). Summer 2022 could be a good time to return.

597

598 Code availability

599 WRF codes used are readily available from <https://github.com/wrf-model/WRF/releases/tag/v4.2.2>. Modifications
600 and additional details are in Cheng et al (2021).

601

602 Author contributions



603 ZC, LC, SA, WW and YC were primarily involved in aspects of the WRF code adaptation and model runs. PAT,
604 GAI and TWB were primarily involved in reviewing background information and interpretation of results. PAT
605 prepared the manuscript with contributions from all co-authors.

606

607 **Competing interests**

608 The authors declare that they have no conflict of interest.

609

610 **Acknowledgements**

611 Financial support for this research, for which we are very grateful, has come primarily through a Canadian NSERC
612 Collaborative Research and Development grant program (High Resolution Modelling of Weather over the Grand
613 Banks) with Wood Environmental and Infrastructure Solutions as the industrial partner. Initial support was also
614 through Peter Taylor's NSERC Discovery grant. We would like to thank Anton Beljaars for providing guidance and
615 many valuable comments as well as Ayrton Zadra and Jason Milbrandt for their help in tracking down details of
616 Environment Canada's GEM model. Trevor VandenBoer pointed us to the aerosol work and Joe Fernando allowed
617 two of us to attend a C-Fog meeting in 2019 where we also had useful discussions with Will Perrie and Rachel
618 Chang.

619

620 **References**

- 621 Alexander C et al (23 co-authors) (2020) Rapid Refresh (RAP) and High Resolution Rapid Refresh (HRRR) Model
622 Development, slides from AMS 100th Annual Meeting, available at [https://rapidrefresh.noaa.gov/pdf/
623 Alexander_AMS_NWP_2020.pdf](https://rapidrefresh.noaa.gov/pdf/Alexander_AMS_NWP_2020.pdf), accessed 24 Jan 2021.
- 624 Barker EH (1977) A maritime boundary-layer model for the prediction of fog. *Boundary-Layer Meteorol* 11: 267-
625 294.
- 626 Belair S, Mailhot J, Girard C and Vaillancourt P (2005) Boundary layer and shallow cumulus clouds in a medium-
627 range forecast of a large-scale weather system. *Mon. Wea. Rev* 133: 1938–1960, doi:10.1175/MWR2958.1.
- 628 Bergot T (1993) Modélisation du brouillard à l'aide d'un modèle 1D forcé par des champs mésoéchelle: Application
629 à la prévision. Ph.D. thesis, Université Paul Sabatier, Toulouse, France, 192 pp.
- 630 Bergot T, Guedalia D (1994) Numerical forecasting of radiation fog. Part I: Numerical model and sensitivity tests.
631 *Mon. Wea. Rev* 122: 1218–1230.
- 632 Bergot T, Carrer D, Noilhan J, Bougeault P (2005) Improved site-specific numerical prediction of fog and low clouds:
633 A feasibility study. *Weather Forecasting* 20: 627–646.
- 634 Bergot T, Terradellas E, Cuxart J, Mira A, Liechti O, Mueller M, Woetmann Nielsen N (2007) Inter comparison of
635 Single-Column Numerical Models for the Prediction of Radiation Fog, *Journal of Applied Meteorology and
636 Climatology* 46: 504–521
- 637 Bott A, Trautmann T (2002) PAFOG—A new efficient forecast model of radiation fog and low-level stratiform clouds.
638 *Atmos. Res* 64: 191–203, [https://doi.org/10.1016/S0169-8095\(02\)00091-1](https://doi.org/10.1016/S0169-8095(02)00091-1).
- 639 Bott A, Sievers U, Zdunkowski W (1990). A radiation fog model with a detailed treatment of the interaction between



- 640 radiative transfer and fog microphysics. *J. Atmos. Sci* 47: 2153–2166.
- 641 Boudala FS, Isaac GA, Crawford R, Reid J (2012) Parameterization of runway visual range as a function of visibility:
642 Implications for numerical weather prediction models. *J. Atmos. Oceanic Technol* 29,:177–191
- 643 Brown R, Roach WT (1976) The physics of radiation fog. II. A numerical study. *Q. J. R. Meteorol. Soc* 102:335–354.
- 644 Brutsaert W (1982) *Evaporation into the Atmosphere: Theory, History, and Applications*. Springer, Dordrecht,
645 <http://dx.doi.org/10.1007/978-94-017-1497-6>
- 646 Burkard R, Eugster W, Wrzesinsky T, Klemm O (2002), Vertical divergences of fogwater fluxes above a spruce forest.
647 *Atmospheric Research* 64:133-145.
- 648 Caffrey PF, Ondov JM, Zufall MJ, Davidson CI. 1998. Determination of size-dependent dry particle deposition
649 velocities with multiple intrinsic elemental tracers. *Environ. Sci. Technol.* 32:1615–22
- 650 Charnock H (1955) Wind stress on a water surface. *Quart. J. Roy. Meteorol. Soc* 81:639-640.
- 651 Chen C, Zhang M, Perrie W, Chang R, Chen X, Duplessis P, Wheeler M (2020) Boundary layer parameterizations to
652 simulate fog over Atlantic Canada waters. *Earth and Space Science*, 7, e2019EA000703.
653 <https://doi.org/10.1029/2019EA000703>
- 654 Cheng, L., Chen, Z. and Chen, Y. (2021) WRF coding notes related to Surface deposition of marine fog, to be posted
655 on the York University Dataverse site.
- 656 de la Fuente L, Delage Y, Desjardines S, MacAfee A, Pearson G, Ritchie H (2007) Can sea fog be inferred from
657 operational GEM forecast fields? *Pure Appl. Geophys* 164:1303–1325.
- 658 ECMWF (2020) IFS Documentation CY47R1, Part IV: Physical Processes,
659 <https://www.ecmwf.int/en/elibrary/19748-part-iv-physical-processes>, accessed 25 Jan 2021
- 660 Farmer D.K., Boedicker, E.K. and DeBolt, H.M., (2021) Dry Deposition of Atmospheric Aerosols: Approaches,
661 Observations, and Mechanisms, *Annu. Rev. Phys. Chem.* 72:16.1–16.23
- 662 Fernando H., Gultepe I, Dorman C, Pardyjak E, Wang Q, Hoch S, Richter D, Creegan E, Gabersek S, Bullock T,
663 Hocut C, Chang R, Alappattu D, Dimitrova R, Flagg, D, Grachev A, Krishnamurthy R, Singh, D, Lozovatsky I,
664 Fernand H (2021) C-FOG: Life of Coastal Fog. *Bulletin of the American Meteorological Society* 102:
665 10.1175/BAMS-D-19-0070.1.
- 666 Forkel R, Sievers U, Zdunkowski W (1987) Fog modelling with a new treatment of the chemical equilibrium
667 condition. *Beitr. Phys. Atmo* 60:340–360.
- 668 Garratt JR (1992) *The Atmospheric Boundary layer*, Cambridge University Press.
- 669 Goodman J (1977) The microstructure of California Coastal fog and stratus. *J. Appl. Meteor* 16:1056–1067.
- 670 Gultepe I, Muller MD, Boybeyi Z (2006) A new visibility parametrization for warm fog applications in numerical
671 weather prediction models. *J. Appl. Meteorol* 45:1469–1480
- 672 Gultepe I, Pearson G, Milbrandt JA, Hansen B, Platnick S, Taylor P, Gordon M, Oakley JP, Cober SG (2009) The
673 Fog Remote Sensing and Modeling (FRAM) field project. *Bull. Amer. Meteor. Soc* 90:341–359.
- 674 Gultepe I, Milbrandt JA, Zhou B (2017) Marine Fog: A Review on Microphysics and Visibility Prediction, in *Marine
675 Fog: Challenges and Advancements in Observations, Modeling and Forecasting*, D. Koračin and C. Dorman,
676 Eds., Springer 345-394.



- 677 Hallett J, Christensen L (1984) Splash and penetration of drops in water. *Journal de Recherches Atmospheriques*
678 18:225–242.
- 679 Isaac GA, Hallett J (2005) Clouds and Precipitation, in *Encyclopedia of Hydrological Sciences*. Edited by M.
680 Anderson.
- 681 Isaac GA, Bullock T, Beale J., Beale S (2020) Characterizing and Predicting Marine Fog Offshore Newfoundland and
682 Labrador. *Weather and Forecasting* 35:347-365
- 683 Katata G, Nagai H, Wrzesinsky T, Klemm O, Eugster W, Burkard R (2008) Development of a land surface model
684 including cloud water deposition on vegetation, *Journal of Applied Meteorology and Climatology*, 47, 2129-2146.
- 685 Katata G, Kajino M, Hiraki T, Aikawa M, Kobayashi T, Nagai H (2011) A method for simple and accurate estimation
686 of fog deposition in a mountain forest using a meteorological model. *Journal of Geophysical Research*
687 116:D20102.
- 688 Katata G (2014) Fogwater deposition modeling for terrestrial ecosystems: A review of developments and
689 measurements, *J. Geophys. Res. Atmos* 119: 8137–8159. doi:10.1002/2014JD021669
- 690 Kim CK, Yum SS (2012) A numerical study of sea fog formation over cold sea surface using a one-dimensional
691 turbulence model coupled with the Weather Research and Forecasting Model. *Boundary Layer Meteorol*
692 143:481–505.
- 693 Kim W, Yum SS, Hong J, Song JI (2020) Improvement of Fog Simulation by the Nudging of Meteorological Tower
694 Data in the WRF and PAFOG Coupled Model. *Atmosphere* 11: 311. doi:10.3390/atmos11030311
- 695 Klemm O, Wrzesinsky T, Scheer C (2005) Fog water flux at a canopy top: Direct measurement versus one-
696 dimensional model. *Atmos. Environ* 39:5375–5386.
- 697 Koracin D, Dorman C, Lewis J, Hudson J, Wilcox E, Torregrosa A (2014) Marine fog: A review. *Atmospheric*
698 *Research* 143:142–175.
- 699 Koračin D (2017) Modeling and forecasting marine fog. in *Marine Fog: Challenges and Advancements in*
700 *Observations, Modeling and Forecasting*, D. Koračin and C. Dorman, Eds., Springer, 425–475
- 701 Kunkel A (1984) Parameterization of droplet terminal velocity and extinction coefficient in fog models. *J. Climate*
702 *Appl. Meteor* 23:34–41.
- 703 Lin C, Zhang Z, Pu, Z and Wang F (2017) Numerical simulations of an advection fog event over Shanghai Pudong
704 International Airport with the WRF model. *Journal of Meteorological Research* 31:874-889.
- 705 Lovett GM (1984) Rates and mechanisms of cloud water deposition to a subalpine balsam fir forest. *Atmos. Environ*
706 18:361–371.
- 707 Maronga B, Bosveld F (2017) Key parameters for the life cycle of nocturnal radiation fog: a comprehensive large-
708 eddy simulation study. *Quart J R Meteorol Soc* 143:2463–2480
- 709 Milbrandt JA, Yau MK (2005) A multimoment bulk microphysics parameterization scheme. Part II: A proposed three-
710 moment closure and scheme description. *J. Atmos. Sci* 62:3065–3081, doi:10.1175/JAS3535.1.
- 711 Milbrandt JA, Bélair S, Faucher M, Vallée M, Carrera ML, Glazer A (2016) The Pan-Canadian high resolution (2.5
712 km) deterministic prediction system. *Weather and Forecasting* 31(6):1791-1816.
- 713 Morrison H, Curry JA, Khvorostyanov VI (2005) A new double-moment microphysics parameterization for



- 714 application in cloud and climate models. Part I: description. *J Atmos Sci* 62(6):1665–1677.
715 <https://doi.org/10.1175/JAS3446.1>
- 716 Morrison H, Milbrandt JA (2015) Parameterization of ice microphysics based on the prediction of bulk particle
717 properties. Part I: Scheme description and idealized tests. *J. Atmos. Sci* 72:287–311, doi:10.1175/JAS-D-14-
718 0065.1.
- 719 Musson-Genon L (1987) Numerical simulation of a fog event with a one-dimensional boundary-layer model. *Mon.*
720 *Weather Rev* 115:29-39
- 721 Olson JB, Kenyon JS, Angevine WA, Brown JM, Pagowski M, Suselj K (2019) A Description of the MYNN-EDMF
722 Scheme and the Coupling to Other Components in WRF–ARW. NOAA Technical Memorandum OAR GSD-61.
723 <https://doi.org/10.25923/n9wm-be49>
- 724 Pinnick R, Hoihjelle DL, Fernandez G, Stenmark EB, Lindberg JD, Hoidale GB, Jennings SG (1978) Vertical structure
725 in atmospheric fog and haze and its effect on visible and infrared extinction. *J. Atmos. Sci* 35:2020–2032.
- 726 Qi J, Yu Y, Yao X, Gang Y, Gao H. 2020. Dry deposition fluxes of inorganic nitrogen and phosphorus in atmospheric
727 aerosols over the Marginal Seas and Northwest Pacific. *Atmos. Res.* 245:105076
- 728 Richter DH, MacMillan T, Wainwright C (2021) A Lagrangian Cloud Model for the Study of Marine Fog. *Boundary-*
729 *Layer Meteorol.*, <https://doi.org/10.1007/s10546-020-00595-w>
- 730 Rogers RR, Yau MK (1989) *A short course in Cloud Physics*, Pergamon, Oxford.
- 731 Schemenauer RS, Cereceda P (1991) “Fog-Water Collection in Arid Coastal Locations.” *Ambio* 20(7):303–308.
- 732 Sehmel G, Sutter S. 1974. Particle deposition rates on a water surface as a function of particle diameter and air velocity.
733 Rep. BNWL-1850, Battelle Pac. Northwest Labs, Richland, WA
- 734 Schwenkel J, Maronga B (2019) Large-eddy simulation of radiation fog with comprehensive two-moment bulk
735 microphysics: impact of different aerosol activation and condensation parameterizations, *Atmos. Chem. Phys*
736 19:7165–7181, <https://doi.org/10.5194/acp-19-7165-2019>.
- 737 Schwenkel J, Maronga B (2020) Towards a better representation of fog microphysics in large-eddy simulations based
738 on an embedded Lagrangian cloud model. *Atmosphere* 11:466. <https://doi.org/10.3390/ATMOS11050466>
- 739 Shuttleworth WJ (1977) The exchange of wind-driven fog and mist between vegetation and the atmosphere.
740 *Boundary-Layer Meteorol* 12:463-489.
- 741 Siebert J, Bott A, Zdunkowski W (1992a) Influence of a vegetation-soil model on the simulation of radiation fog.
742 *Beitr. Phys. Atmos* 65:93–106.
- 743 Siebert J, Sievers U, Zdunkowski W (1992b) A one-dimensional simulation of the interaction between land surface
744 processes and the atmosphere. *Boundary-Layer Meteorol* 59:1–34.
- 745 Skamarock WC, Klemp JB, Dudhia J, Gill DO, Liu Z, Berner J, Wang W, Powers JG, Duda MG, Barker DM, Huang
746 X-Y (2019) A Description of the Advanced Research WRF Model Version 4 (No. NCAR/TN-556+STR).
747 doi:10.5065/1dfh-6p97
- 748 Stolaki S, Pytharoulis I, Karacostas T (2012) A study of fog characteristics using a coupled WRF-COBEL model over
749 Thessaloniki Airport, Greece. *Pure and Applied Geophysics* 169:961-981.
- 750 Taylor GI (1917) The formation of fog and mist. *Quart. J. Roy. Meteor. Soc* 43:241–268, <https://doi.org/10.1002/>



751 qj.49704318302.
752 Taylor PA, Salmon JR, Stewart RE (1993) Mesoscale observations of surface fronts and low pressure centres in
753 Canadian East Coast winter storms. *Boundary-Layer Meteorol* 64:15–54. <https://doi.org/10.1007/BF00705661>,
754 Teixeira J (1999) Simulation of fog with the ECMWF prognostic cloud scheme. *Quarterly Journal of the Royal*
755 *Meteorological Society*,125(554):529-552
756 Tiedtke M (1993) Representation of clouds in large-scale models. *Mon. Weather Rev* 121:3040-3061
757 Wainwright C, Richter D (2021) Investigating the Sensitivity of Marine Fog to Physical and Microphysical Processes
758 Using Large-Eddy Simulation. *Boundary-Layer Meteorol*. <https://doi.org/10.1007/s10546-020-00599-6>
759 Williams, R. M. (1982) A model for the dry deposition of particles to natural water surfaces, *Atmos. Environ.* 16,
760 1933-1938.
761 Wilkinson JM, Porson ANF, Bornemann FJ, Weeks M, Field PR, Lock AP (2013) Improved microphysical
762 parametrization of drizzle and fog for operational forecasting using the Met Office Unified Model. *Quart. J. Roy.*
763 *Meteor. Soc* 139:488–500, <https://doi.org/10.1002/qj.1975>
764 WMO (2020) Variable: Meteorological Optical Range (MOR) (surface) accessed 4 Jan 2021, [https://www.wmo-](https://www.wmo-sat.info/oscar/variables/view/meteorological_optical_range_mor_surface)
765 [sat.info/oscar/variables/view/meteorological_optical_range_mor_surface](https://www.wmo-sat.info/oscar/variables/view/meteorological_optical_range_mor_surface)
766 Yang D, Ritchie H, Desjardins S, Pearson G, MacAfee A, Gultepe I (2010) High-Resolution GEM-LAM Application
767 in Marine Fog Prediction: Evaluation and Diagnosis, *Weather and Forecasting* 25:727–748
768 Yang Y, Gao S (2020) The impact of turbulent diffusion driven by fog-top cooling on sea fog development. *Journal*
769 *of Geophysical Research: Atmospheres*,125:e2019JD031562. <https://doi.org/10.1029/2019JD031562>
770 Zdunkowski WG, Barr AE (1972) A Radiative-Conductive Model for the Prediction of Radiation Fog. *Boundary-*
771 *Layer Meteorol* 3:152-177
772 Zhou B, Du J (2010) Fog Prediction from a Multimodel Mesoscale Ensemble Prediction System, *Weather and*
773 *Forecasting* 25(1):303–322. <https://doi.org/10.1175/2009WAF2222289.1>
774 Zufall MJ, Davidson CI, Caffrey PF, Ondov JM. 1998. Airborne concentrations and dry deposition fluxes of
775 particulate species to surrogate surfaces deployed in southern Lake Michigan. *Environ. Sci. Technol.* 32:1623–
776 28
777 -----